Properties of sands of different geological origins in mortars

Tchedele Langollo Yannick (yannicktl@yahoo.com)
Local Materials Promotion Authority (MIPROMALO)
Bilkissou Alim
Local Materials Promotion Authority (MIPROMALO)
Abdou Nasser Njoya Mfokou
National Institute of Cartography (INC)
Oumar Ali Taïga
Local Materials Promotion Authority (MIPROMALO)
Njoya Moussa Jalil
University of Ngaoundere
Belinga Essama Boum Raphael
Local Materials Promotion Authority (MIPROMALO)
Mache Jacques Richard
University of Ngaoundere

Research Article

Keywords: sand, mortar, strength, setting time, formulation, mineralogy

Posted Date: April 4th, 2022

DOI: https://doi.org/10.21203/rs.3.rs-1508892/v1

Properties of sands of different geological origins in mortars

Tchedele Langollo Yannick[a,b], Bilkissou Alim[a,b], Njoya Mfokou Abdou Nasser[c], Oumar Ali Taïga[a], Njoya Moussa Jalil[b], Belinga Essama Boum Raphael[a], Mache Jacques Richard[d]

a) Research Department, Local Materials Promotion Authority (MIPROMALO), Yaounde, Cameroon.
b) Department of Mining Engineering, School of Geology and Mining Engineering, University of Ngaoundere, Meiganga, Cameroon.

c) National Institute of Cartography (INC), Yaounde, Cameroon.

d) Laboratory of Clays, Geochemistry and Sedimentary Environments (AGEs), Boulevard du Rectorat, 17 (Bât. B18) Sart Tilman – 4000, Liege, Belgium.

Correspondence to: yannicktl@yahoo.com

Abstract

This work is a comparative study between sand mortars of different geological origins, intending to highlight their influence on mortar properties. For this purpose, five sand types and the cement CEM II/B-P 42.5R were used for the formulation of mortars with identical W/C ratios. These are the "Sanaga" sand from the Sanaga River, the "Wouri" sand from the Wouri River, the Nyambaka basalt sand, the Meiganga granite sand, and the Leboudi gneiss sand. These sands were characterized and classified according to their physical, chemical, and mineralogical properties. They were then used to make mortars. From the results of the setting time tests carried out on the mortars, it appears that the initial setting time varies from 195 min for MS04 to 210 min for MGN03, while passing by MW05 (200 min), MB01 (198 min), and MGR02 (196 min). The final setting time varied from 496 min (MGR01) to 510 min (MGN03) with an average of 300 min over and above the initial setting time to reach the final setting time. The flexural strength tests of the mortars show that the crushed sands have better properties than the alluvial sands. They vary from 1.64 to 2.18 MPa at 2 days, from 3 to 3.90 MPa at 7 days, and from 7 to 14.84 MPa at 28 days. As for the compressive stress tests, the results show that the quarry sand mortars studied have higher average compressive strengths than the alluvial sand mortars, with basalt sand offering the best performance. These strengths range from 6.35 to 10.83 MPa at 2 days, 7.55 to 18.96 MPa at 7 days, and 22.81 to 34.58 MPa at 28 days, with 34.58 MPa for the basalt mortar. The mineralogical

analysis of the mortars reveals the presence of cement hydrates and non-hydrated phases in all the mortars. They also show the absence of minerals brought by the sands that could chemically interfere in the setting process.

Keywords: sand; mortar; strength; setting time; formulation, mineralogy

1. Introduction

The world is in full demographic expansion, this expansion generates many challenges because it is accompanied by increased demand for goods and services. Therefore, the construction of sustainable infrastructure is essential for the well-being of the population, and to achieve this, the production of aggregates is essential. With the realization of more and more gigantic works, the requirements on the intrinsic properties of the materials are growing. With a diversified offer, natural aggregates are obtained by the exploitation of quarries in different geological contexts which could influence the quality of the produced materials.

The mortar is made up of an assembly of materials of a generally mineral nature (cement, sand), its setting and hardening are mainly due to the formation of the various hydrates of the cement caused by the hydration of the various mineral phases in presence as well as the intrinsic properties of the sand used [1,2].

One of the essential properties of mortar is its ability to conform to the shape into which it is poured while still in a fresh state. Its implementation depends on the setting time, which is the time it takes for the concrete to support the loads induced by its weight without deformation [3]. The mechanical behavior of mortars depends strongly on their microstructure, the quality of the matrix-aggregate interface, and the size, orientation, and density of the elements that constitute it [4- 6].

Despite numerous research works carried out on mortars [7-10], questions remain unanswered concerning the interaction between cement and aggregates, especially those concerning the influence of the nature of the aggregates on the hydration phenomenon. From this point of view, works [11] have shown that the mechanical properties of mortars based on quarry sand were close to each other and that mortars based on alluvial sands presented weaker mechanical properties than the latter. Thus, to further investigate this line of research, especially

concerning the causes of the disparities observed in the mechanical resistances, it is relevant to study the influence of the geological origin of the sands on the formation of the hydrates of the cement, through the characterization of the aggregates and the study of the setting time of mortars. Subsequently, to evaluate their impact on the hardening through the determination of mechanical resistance.

To do this, we will be interested in the chemical, physical, and mineralogical characterization of the sands, the determination of setting times, flexural and compressive tensile strengths, and mineralogical properties of mortars in the fresh and hardened state as appropriate.

2. Location of the study area

The geographical location of the sand collection sites used in this study is presented here. Figures 1 and 2 present maps of the location of the study areas in different regions of Cameroon. Table 1 summarizes the coordinates of the sampling sites.

3. Geology of the sampling sites

3.1. The basalt

The basalt was collected at Nyambaka, a commune at coordinates [N6°53'29" E14°05'43"] in the Adamaoua region, Vina department.

The Nyambaka area is covered essentially by volcanic rocks. These volcanic rocks are mainly an ancient series of basalt-andesite [12]. According to Toteu et al [13], the Nyambaka area is essentially made up of rocks of Cenozoic volcanic-plutonic origin.

3.2. The granite

The granite block used in our study was taken from the abandoned quarry of a road project. It is located in Dana, Meiganga which is a town located at coordinates [N6°30'55" E14°17'29"] in the Adamaoua region and chief town of the Mbéré department.

The Meiganga area is made up of magmatic rocks, metamorphic rocks, and sedimentary rocks [14, 15]. According to the geological reconnaissance map of Cameroon [12], the southern part of Meiganga in which the study site is located is covered mainly by two types of geological formations, these are metamorphic and plutonic formations. The metamorphic formations are

represented by the rocks of the Lom series, the base complex, and the gneisses. The magmatic or plutonic formations constitute the dominant geological formation [12, 13]. They are syntectonic concordant granites constituted among others by calc-alkaline granites with biotite, biotite, amphibole, and pyroxene. The Dana area (sample site) is mainly composed of undifferentiated granites with porphyritic texture. These granites are cut by intrusions represented by SW-NE-oriented quartz veins and SE-NW-oriented microgranite veins [12].

3.3. The gneiss

The gneiss sand is produced by CHINA MEILAN CAMEROON COMPANY SARL (CMCC), whose exploited massif is located at the coordinates [**N3°53'51'' E11°26'57''**] in the central region, department of lekié, in the district of Okola, more precisely in the locality of Leboudi

In the area of southern Cameroon where the study area is located, studies highlight a bedrock consisting mainly of metamorphic and plutonic rocks belonging to the Precambrian base complex [16, 17, 18]. The basement of southern Cameroon is composed of two major petrostructural groups: the Ntem Group and the Yaoundé Group. The Yaoundé Group is a very homogeneous group resulting from the high-pressure metamorphism of a geological material of volcanic-sedimentary origin. It consists of the Yaoundé and Mbalmayo-Bengbis series [18]. The

The Yaoundé series is a unit that outcrops essentially in the Yaoundé region. It is made up of formations of the Pan-African chain of age 540-600 Ma. These formations belong to the ancient metamorphic basement of the Cameroon Base Complex [16] consisting of paraderivorous and orthoderivorous formations. The latter are intrusive in the paraderivative formations. The paraderivative metamorphites are composed of various paragneisses, micaschists, and simple quartzite and disthene in low proportion while the orthoderivative formations which were sampled, are formed of pyroclasts (pyroxene and plagioclase gneiss) to which are associated pyroxene and amphibole gneiss, pyroxenites, and biotites [19].

3.4. Sanaga sand

The sand of the Sanaga River is collected on a site of artisanal extraction in Ebebda at the coordinates [N4°22'00" E11°16'03"], which is a commune of Cameroon located in the region of the center and the department of the lekié.

The geology of the Sanaga watershed is constituted by a basic complex formed by a large set of crystalline shales made up of ectinites, migmatics, and concordant ancient eruptive rocks represented essentially by syntectonic granites. We also note the formation of lower micaschists and quartzites with constant facies; we also note the same folding directions without forgetting the presence of the upper and lower gneiss towards the banks of the river [20].

I.2.4 Wouri sand

The sand from the Wouri River used in this study was taken from an artisanal extraction site in Bonamoussadi in the littoral region, Wouri department, Douala 5th district. The sand was extracted from the Bonamoussadi beach quarry at coordinates [N4°06'15" E9°44'05"].

The part of the Wouri River sampled has a geological cover constituted by the formations of the basement essentially represented by gneiss-embrechists with biotite and secondarily by anatexis, syntectonic granites not circumscribed and circumscribed [21].

4. Materials and Methods

4.1. Materials

4.1.1. Sands

The sampling of sands was carried out following **NF EN 932-1, 1996** Standard. During this stage, three (03) samples of sands were taken in the granular state, namely the alluvial sand of the Sanaga River at Ebebda - Monatélé (SS05), the alluvial sand of the Wouri River at Bonamoussadi - Douala (SW04), and the gneiss sand coming from the quarry of Leboudi in Yaoundé (SGN03). Two (02) additional sand samples were taken from granite blocks collected in Meiganga and Basalt blocks collected in Nyambaka. These were crushed with a sledgehammer and then ground and sieved in the laboratory to retain the 0.08/2 mm particle size class**.**

4.1.2. Cement

The choice of the cement to be used was the ROBUST 42.5R type NC CEM II/B-P 42.5R of the company CIMENCAM SARL in Figuil because it is the most used in Cameroon. It complies

with the Cameroonian standard NC 235:2005. The characteristics of the cement are summarized in Table 2:

4.2. Methods

4.2.1. Sand preparation

The preparation of the mortar specimens was subject to the preparation of the sands in the laboratory in the following steps: The blocks of rocks taken from the field were crushed with a sledgehammer and an anvil; the rock fragments were passed through a ball mill; the products of the crushing and the alluvial sands were dried and then passed through a 2mm sieve and the bypasses were kept; these by-passes were then washed with a 0.080 mm sieve to eliminate the fine clayey materials, plant materials and thus avoid the agglomeration of the grains, which could distort the results of the analysis. The final step consisted in drying each sand sample in an oven at 105°C for 24 hours.

4.2.2. Particle size analysis by sieving

The granulometric analysis allows determining the size and the respective weight percentages of the different families of grains constituting the sand sample. This test is defined by the standards EN 933-1 and EN 933-2. The following formulas were used in the context of the realization of this test: **1**

- Percentage of cumulative sieves P (%):

$$\mathbf{P\ (\%) = 100 - r\ (\%)} \qquad \mathbf{(1)}$$

- The percentage of cumulative refusals for each sample type is denoted r (%) and is determined as follows: $\mathbf{r(\%) = (R/M) \times 100}$ **(2)** With :

R: the mass of accumulated refusals in grams.

M: the mass of the test sample for each sample

4.2.3. Sand equivalent according to the NFP 18-598 standard

This test measures the cleanliness of the sand. It gives an overall account of the quantity and quality of the fine elements, by expressing a conventional volumetric ratio between the sandy

elements that sediment and the fine elements that flocculate. The visual sand equivalent (VSE) is defined by the formula **(2)**:

$$\mathbf{ESV} = \frac{\boldsymbol{h}}{\boldsymbol{h1}} \times \mathbf{100} \qquad \textbf{(2)}$$

The sand equivalent (ES) is defined by formula **(3)**:

$$\mathbf{ES} = \frac{\boldsymbol{h2}}{\boldsymbol{h1}} \times \mathbf{100} \qquad \textbf{(3)}$$

With:

$\boldsymbol{h1}$: the height of the upper level of the flocculate about the bottom of the test tube.

$\boldsymbol{h2}$: the height of the top level of the sedimented portion relative to the bottom of the specimen.

$\boldsymbol{h}$**:** the height of the sediment at the level of the upper face of the sleeve.

4.2.4. Densities

4.2.4.1. The absolute density according to the NFP 18-301 standard

The purpose of this test is to determine the mass per unit volume of the material that constitutes the aggregate without taking into account the voids that may exist between the grains. The absolute density is determined by the formula **(4)**:

$$\boldsymbol{\rho} = \frac{\boldsymbol{v2}-\boldsymbol{v1}}{\boldsymbol{M}} \qquad \textbf{(4)}$$

With:

$\boldsymbol{\rho}$: Absolute density

$\boldsymbol{M}$ Mass of solid grains (about 300g)

$\boldsymbol{v1}$Volume of water

$\boldsymbol{v2}$Total volume (solid grains + water)

4.2.4.2. The apparent density according to the NF P 18-554 standard

It allows to obtain the mass of the apparent volume unit of the body, that is to say, the volume constituted by the material of the body and the voids it contains. The apparent density is determined by the formula **5**:

$$\boldsymbol{\rho} = \frac{\boldsymbol{M1-M0}}{\boldsymbol{v}} \qquad \textbf{(5)}$$

With:

$\boldsymbol{\rho}$: Bulk density

$\boldsymbol{M1}$: Mass of the filled container (container + sand)

$\boldsymbol{M0}$: Mass of the empty container

$\boldsymbol{v}$: Volume of the container

4.2.5. Petrography

Thin sections are made at the Institute for Mining and Geological research of (Yaoundé, Cameroon). Microscopic observations are done under a polarized microscope of brand LEITZ WETZLAR observed at the laboratory of Petrology and Magmatism of the Geosciences of Deep Formations and Applications, University of Yaounde I.

4.2.6. X-Ray Fluorescence Spectrometry (XRF)

For XRF analysis, a hXRF Niton XL3t980 analyzer (equipped with an Ag-Anode 50 kV X-ray tube and Silicon-Drift-Detector 8 mm spot was used. The raw data were plotted in spectra, where x-axes represent element-specific fluorescence energy (unit keV), and y-axes quantify counts of photons (unit cps) received by the detector. Detection is possible for most of the elements with atomic numbers ranging from 12 Magnesium to 92 (Uranium). A 21 silicon-based standards so-called Certified Reference Material (CRM), filled in cups and covered with 4 µm polypropylene film were measured by hXRF device-specific mode (mining/mineral mode). The measured values were plotted using a trend line equation and the "fitting coefficient" R^2 (correlation coefficients) were determined. Afterward, a classification was made according to the quality of the regression line and the distribution of the data. XRF was performed on the different sands.

4.2.7. Production of mortar samples

The mortar samples were made according to EN 196-1 with dimensions of 4x4x16 cm. From the formulation of the normal mortar, at w/c=0.5, the sand used was basalt sand (SB01), granite sand (SGR02), gneiss sand (SGN03), Canada sand (SS04), and wouri sand (SW05). The

different formulations were MB01, MGR02, MGN03, MS04, and MW05 respectively for each sand used. Three samples of each formulation were used for both the flexural strength test and compressive strength test. A total of 45 prismatic mortar specimens were produced. The quantities used are found in Table 3.

4.2.8. Setting time

The setting time test is performed with the Vicat apparatus on the cement paste at normal consistency. The initial setting time is the time from the beginning of mixing of the cement paste until the Vicat needle is stopped at a distance d from the bottom of the mold loaded with 500g of paste and such that d = 4 ± 1 mm. The final setting time is the time after which the end of setting time needle only sinks by 0.5 mm. This test is carried out following Standard EN 196-3.

4.2.9. Mechanical tests

The flexural strength test was carried out on three 4x4x16cm prismatic mortar specimens, for each formulation, at 2, 7, and 28 days of cure. In the end, the strength allowed is the average of the three values obtained. This test is performed according to EN 196-1 using the formula (5):

$$R_t = \frac{1{,}5 \times P \times L}{b^3} \qquad (5)$$

Where R_t = Flexural Strength MPa
L = distance between the lower support in mm
P = breaking load in N
b = thickness of the specimen (b = 40 mm)

The compressive strength test is carried out on each half of the specimen used for the flexural test at the same dates, following NF-P-15-301 and ENV 197-1. The strength allowed is also the average of the values obtained. The compressive strength is calculated using the formula (6):

$$R_c = \frac{P}{S} \qquad (6)$$

With R_c = compressive strength MPa
P = breaking load N
S = specimen section in mm^2 (S = 1600 mm^2)

4.2.10. X-Ray Diffractometry (XRD)

XRD measurements were performed using a D8 Brucker –AXS diffractometer equipped with Lynx eye position-sensitive detector, with Cu Kα ʎCu = 1.54056 Å radiation operated at 40 kV and 40 mA, increment 0.013° 2Θ, and a measuring time per step of 30 s. The diffraction patterns were collected in the 2 theta range from 7.5– 90°. Qualitative analysis of the phase composition of the powder samples was conducted using the PDF-2 2007 release software and X'Pert High Score Plus. XRD was performed on the raw materials (sands) at first and on the mortars, after 2, 7, and 28 curing days, to identify the hydrated products.

5. Résultats et discussions

5.1. Granulometric analysis by sieving and sand equivalent

The results of the particle size analysis of the different sands studied are presented by the particle size curves in Figure3. These results have been reduced to the granular class 0/2.

At the end of this test, it emerges that the sands having undergone a grinding in the laboratory such as granite and basalt present a uniform granulometry with percentages of fine (<0.2mm) included between and20 25% higher than that of the standardized sand. This is due to the grinding process used which mobilized a ceramic ball mill and an identical grinding time, thus conferring them a continuous granulometry with a majority of coarse sands (≥ 0.2 mm) which are nevertheless close to the normalized sand. It should be noted, however, that the basalt shows slightly better resistance to grinding, which suggests a better hardness of the material.

The gneiss quarry sand has a proportion of fines of around 30%. The curve which has a more or less rectilinear aspect from 400 µm, has a continuous granulometry in the whole but presenting a granularity with a majority of average grains (between 0.3 and 1 mm). This sand contains more fine materials than the standardized sand up to the mesh size of 1.52 mm.

Alluvial sands have overall finer grain sizes than quarry sands and standard sand (in the 0.4 and 2mm classes). However, the fine fraction (<0.2mm) represents less than 5% of these sands. Their curves are the most distended of the standard sand.

The determination of the modulus of fineness and the equivalent of sand ES of each sand is reported in table 4.

All the sands studied have a modulus of fineness within the range of permissible values (i.e., between 1.8 and 3.2) according to EN 12620. According to this standard, the Basalt (SB01), Granite (SGR02), and Gneiss (SGN03) sands are said to be a little too fine; While the Sanaga and Wouri sands are classified as coarse sands. These lower fine contents are probably due to the transport of the grains by water, resulting in a gravimetric separation that is to the advantage of the medium to coarse grains during formation in the river beds, but they may also be because they are mainly composed of quartz (hard and unalterable mineral).

The values of the equivalent of the sands of all the sands respect the specifications of the sands to be used in the confection of the quality concretes according to the standard NF EN 933 8 which must be higher than 65%. Also, according to this criterion, they are all considered as very clean sands.

5.2. Absolute density and bulk density

Table 5 summarizes the densities of the rock samples in the natural state.

These results show that the absolute density of quarry sands is higher than that of alluvial sands. The same is true for the bulk density. Basalt has the highest absolute density with 2.87 g/cm^3 followed by Granite (2.71 g/cm^3) and Gneiss (2.63 g/cm^3). The Sanaga sand (2.68 g/cm^3) is denser than the Wouri sand (2.55 g/cm^3). Except for the Wouri sand, the density of all the sands is higher than the minimum threshold of 2.6 g/cm^3 prescribed by the ASTM C118 standard. These results are similar to those of Mambou et al [4] who used Basalt sands of 2.87 g/cm^3 and river sands of 2.60 g/cm^3. However, they diverge from those of Kumar Gupta and Ashok Kumar [7] who used river sands denser (2.65 g/cm^3) than granite powder (2.46 g/cm^3) probably due to the granularity. The results obtained depend on the minerals present in the materials. The denser sands suggest a high content of minerals such as quartz (2.6 5g/cm^3), muscovite (2.8 g/cm^3), albite (2.6 g/cm^3), anorthite (2.5-2.8 g/cm^3), olivine (3.2-3.6 g/cm^3) among other minerals commonly present in Granites, Basalts, and Gneisses.

5.3. Pétrographie of rock samples

5.3.1. Basalt

Two basalt facies (LAME B and LAME C1) were identified among the basalts used (figure 4). For sample LAME B, this rock has a microlithic porphyritic texture with 80% of the rock mass made up of microlites of constitutive minerals to form the matrix. The rock is made up of phenocryst, microphenocrysts, and microlites of olivine, clinopyroxenes, and plagioclases. There is also an abundance of oxides which add up to the constitutive minerals to form the matrix. Olivine crystals in the rock exist as sub-automorphic to xenomorphic phenocrysts, microphenocrysts, and microlites. They are pleochroic; the phenocrysts show cracks. Clinopyroxenes are found as microphenocrysts and microlites in the matrix. They are xenomorphic and measure less than 0.1mm in diameter. They also present an advanced state of alteration. Plagioclases are the most abundant mineral phases in this matrix and are found as needle-like microphenocrysts and microlites. Most of the crystals show the Carlsbad twin and are pleochroic between the grey and white shades of the first order. Oxides are present in the rock as opaque minerals and are also relatively abundant. They are found in the matrix as well as in some mineral phases indicating the impact of alteration.

Regarding the LAME C1 sample, this rock is mesocratic (dark in color). It has a microlithic porphyritic texture and contains more volcanic glass than developed mineral phases. It contains very little olivine and clinopyroxene but is rich in plagioclases, volcanic glass, and oxides. Plagioclases are abundant in the rock and are found as phenocrysts in the form of elongated baguettes and also as needle-like microphenocrystals. The phenocrysts present several cracks through them and have undergone a little bit of alteration. Most of the plagioclases show Carlsbad twins. Clinopyroxenes are less abundant in the rock and are found in phenocrysts and microlites. The phenocryst is sub-automorphic and shows signs of alteration. Olivine in this rock is found as microlites in the groundmass. The oxides here are large and are abundant. They are found both in the groundmass and some phenocrysts.

5.3.2. Granite

Regarding the granite, 3 thin sections (LAME A, LAME I, LAME H) taken from various granite facies were observed (figure 5). Sample LAME A shows that this granitic rock is leucocratic, with more than 70% white minerals. It has a porphyritic texture with large xenomorphic crystal phases. The rock is made up of plagioclase feldspars, potassic feldspars (orthoclase), quartz, and biotite. Plagioclase is abundant in the rock and is found as xenomorphic

phenocrysts. Most crystal phases are pleochroic. The potassic feldspar which is orthoclase is xenomorphic. Quartz is not as abundant as the feldspars and it is also xenomorphic. The biotite crystals are found in clusters.

Sample LAME I has a porphyritic texture. The mineral phases identified are plagioclase, quartz, biotite, and pyroxene. Plagioclase is the most abundant occurring as xenomorphic crystals with a majority of these crystals exhibiting polysynthetic twins. Quartz is found showing a little bit of alteration and some crystals having oxide inclusions. The biotite crystals are found in clusters. Pyroxene is found dotted in the rock with crystals sizes ranging between 1 to 5mm long.

The sample LAME H presents the same characteristics as the other granitic rock except that it is dominated by light minerals and has muscovite which presents itself as a phenocryst.

5.3.3. Gneiss

The LAME F and LAME G samples observed in figure 6 for the Gneiss show that the rock is foliated and dominated by light minerals while the other rocks do not show any distinctive direction of mineral orientation. All rocks contain quartz, plagioclase, biotite, and muscovite; the rock has the highest proportion of muscovite and biotite. Plagioclases in all rocks exhibit polysynthetic twins with rock F having other plagioclases exhibiting the Carlsbad twin.

5.4. Résultats de l'analyse chimique par fluorescence au rayon X

Table 6 shows the chemical composition of the sands studied.

The Loss On Ignition (LOI) varies from 1.12 to 1.87. Concerning alluvial sands, it is from 1.55 for Sanaga sand to 1.87 for Wouri sand. Quarry sands have losses with 1.65 for basalt, 1.37 for granite, and 1.12 for gneiss. These values correspond to the presence of organic matter in the various materials and can be considered as meeting the ASTM C40 standard.

The different materials are characterized by high silica contents that vary between 41.27 and 63.19% with an arithmetic average of 52.75%. The highest contents are found among the alluvial sands whose values vary from 61.78% for the Wouri sand to 63.19% for the Sanaga sand. These silica contents are because the basement of the Sanaga basin is constituted by a basic complex formed by crystalline schists made up of ectinite, magmatic and syntectonic granites, lower micaschists, and quartzites with constant facies [20]. The basement of the Wouri basin is

essentially represented by biotite gneiss-embrechists and secondarily by anatexis, uncircumscribed, and circumscribed syntectonic granites [21]. These rocks have for main constituent the quartz which is a mineral of hardness 7 according to the scale of Mohs, this last one will thus resist the alteration during the transport. The quarry sands have silica contents that vary from 41.27 to 55.18%. The highest content is that of granitic sand usually rich in quartz, its silica content is 55.18%.

For the other major oxides, the alumina content varies between 5.4 and 11.96%. Quarry sands show an alumina concentration between 9.68 and 11.96%, the highest value being in granite. The alluvial sands show contents that oscillate around 5.4 to 5.83%, the highest value being that of the Sanaga sand. These values are due to the presence of feldspars and potentially Kaolinite in the materials. Iron oxide contents vary from 3.01 to 12.68%, they could be contributed by olivine and amphiboles. The content of calcium oxide varies from 1.45 to 9.66% probably from calcite, the content of magnesium oxide varies between 0.33 and 17.54% brought by illite and olivine. The other major elements, namely potassium oxide, phosphorus oxide, and sodium oxide, show low concentrations, sometimes less than 1%. These results are similar to those of Elat et al [8] for gneiss and alluvial sands, those of Uncik and Kmecova [22] for Basalt, and those of Kumar and Ashok [7] for granite.

5.5. Résultat de la DRX sur les sables

Le Diffractométrie réalisée sur chaque échantillon de sable étudié a été compilée dans la figure 7.

The diffractogram obtained for the Basalt sample (SB01) allowed the identification of major elements such as quartz (3.34 Å; 2.45 Å; 2.28 Å; 2.23 Å; 2.12 Å; 1.97 Å; 1.81 Å; 1.79 Å; 1.67 Å; 1.45 Å; 1.42 Å; 1.37 Å), illite (10.23 Å; 4.98 Å; 4.44 Å; 3.89 Å; 3.34 Å; 3.20 Å; 2.45 Å; 1.49 Å), pyroxene specifically hyperstene (10.23 Å; 4.03 Å; 2.97 Å; 2.88 Å; 2.12 Å; 2.03 Å; 1.97 Å), plagioclase through albite (3.50 Å ; 1.82 Å) and Anorthite (4.68 Å; 3.75 Å; 3.20 Å; 3.12 Å; 2.95 Å; 2.52 Å), amphibole mainly anthophyllite (10.23 Å ; 3.63 Å; 1.50 Å), calcite (3.89 Å, 2.28 Å; 2.10 Å; 1.92 Å; 1.88 Å; 1.62 Å; 1.52 Å; 1.50 Å; 1.42 Å ; 1.35 Å), olivine which is represented by Antigorite (6.43 Å; 5.15 Å; 2.60 Å; 2.21 Å) and trace elements with analcime (5.59 Å; 3.42 Å; 1.35 Å), wollastonite (2.35 Å; 1.75 Å; 1.72 Å), tridymite (2.77 Å; 2.30 Å). These minerals are commonly referred to as Basalts in the literature [23,24].

The granite analysed includes quartz (4.24 Å; 3.34 Å; 2.45 Å; 2.28 Å; 2.12 Å; 1.97 Å; 1.81 Å; 1.67 Å; 1.60 Å; 1.54 Å; 1.45 Å; 1.37 Å), muscovite (10.09 Å ; 3.34 Å; 2.85 Å; 2.56 Å), pyroxene specifically hyperstene (4.03 Å; 2.51Å; 2.12 Å), plagioclase through albite (3.86Å; 3.60 Å; 3.20 Å) and anorthite (3.75 Å; 3.20 Å; 3.12 Å ; 1,81Å), amphibole mainly anthophyllite (3.05 Å; 1.50 Å), calcite (1.92 Å; 1.88 Å; 1.62 Å; 1.57 Å; 1.50 Å; 1.48 Å; 1.42 Å), vermiculite (14.19 Å; 7.13 Å; 3.55 Å ; 2.21 Å) and trace elements with analcime (5.59 Å; 2.9Å), actinolite (8.41 Å), orthoclase (3.47 Å; 3.24 Å; 2.76 Å; 2,16 Å), kaolinite (2.33 Å; 1.58 Å; 1,48 Å), microcline (2.62 Å). The minerals detected correspond to those obtained by [25,26].

In the gneiss, XRD showed the presence of quartz (4.24 Å; 3.34 Å; 2.45 Å; 2.28 Å; 2.23 Å; 2.12 Å; 1.97 Å; 1.81 Å; 1.79 Å ; 1.67 Å; 1.63 Å; 1.60 Å; 1.54 Å; 1.45 Å; 1.42 Å; 1.37 Å), Muscovite (10?09 Å; 3.34 Å; 2.78 Å; 2.01 Å), Augite (2.90 Å; 2.52 Å; 2.16 Å ; 2.01 Å), plagioclases through albite (3.19 Å) and Anorthite (4.03 Å; 3.75 Å; 3.20 Å), calcite (3.03 Å, 2.51 Å; 2.27 Å; 1.92 Å; 1.88 Å ; 1.62 Å; 1.60 Å) and trace elements with actinolite (4.88 Å), diaspore (3.21 Å; 2.35 Å; 2.13 Å; 1.81 Å), microcline (3.47 Å; 2.62 Å). The works consulted on gneiss [27, 28] correspond to these results.

The Sanaga sand contains quartz (4.25 Å; 3.34 Å; 2.45 Å; 2.28 Å; 2.23 Å; 2.12 Å; 1,99 Å; 1.81 Å; 1.67 Å; 1.54 Å; 1.45 Å; 1.37 Å), illite (3.34 Å; 2.55 Å; 2.24 Å), muscovite (4.95 Å; 3.35 Å ; 3.18 Å; 2.23 Å; 1.99 Å), calcite (3.85 Å, 3.01 Å; 2.82 Å; 2.28 Å; 2.12 Å; 1.92 Å; 1.54 Å, 1.45 Å; 1.37 Å) and trace elements with microcline (2.62 Å), albite (3.85 Å), augite (2.90 Å; 2.01 Å), orthoclase (2.76 Å). The work carried out on the Sanaga sand [29] confirms these results. These minerals are the result of the alteration of the constituent rocks of the Sanaga basin [20].

The Wouri sand contains quartz (4.26 Å; 3.34 Å; 2.45 Å; 2.28 Å; 2.23 Å; 2.12 Å; 1.99 Å; 1.81 Å; 1.67 Å; 1.54 Å; 1.42 Å; 1.37 Å), muscovite (4.95 Å; 3.35 Å; 3.18 Å; 2.78 Å; 2.23 Å; 1.99 Å; 1.66 Å), calcite (2.78 Å; 2.23 Å; 1.99 Å; 1.66 Å), calcite (3.03 Å; 2.45 Å; 2.27 Å; 1.92 Å; 1.88 Å; 1.45 Å; 1.42 Å), and trace elements with kaolinite (2.28 Å; 1.48 Å), microcline (3.47 Å; 3.24 Å; 2.62 Å). These minerals, which are generally found in river sands in Cameroon [30], come from the alteration of rocky materials in the Wouri basin [21].

5.6. Setting time results

The results of the setting test are shown in Figure 8.

The setting time varies from 195 min for MS04 to 210 min for MGN03, via MW05 (200 min), MB01 (198 min), and MGR02 (196 min). As for the end of set time, it varies from 496 min (MGR01) to min510 (MGN03) with an average of 300 min additional to the initial setting time to reach the final setting time. These results are relatively close, except for the Gneiss mortar, which is distinguished by, among other things, sand with the highest content of particles ≤ 500 µm (Figure 3). Numerous works [31,32,33, 34] report that particle size plays a central role in the setting time of mortars, provided that the sands used do not contain chemical elements that may accelerate or retard the setting. Indeed, the Incorporation of recycled fine aggregate into the mortar increases the initial from 20% to 63% depending upon the size fraction of recycled fine aggregate, whereas the final setting time of the mix varies from low to high depending upon the presence of organic matter, clay, etc [31,32]. Resende et al [33] reported that copper slag-based mortar shows delayed setting time i.e., initial and final setting time is increased by 2, 5, 10 h and 3, 8 and 18 h for 25, 50, and 75% substitution respectively. [34] studied the variation in setting time of mortar using natural water, sulphuric acid solution, and hydrochloric acid solution treated recycled fine aggregate. They found that initial, as well as final setting time, decreases due to acid treatment. This reduction in setting time is due to the presence of calcium chloride residue and calcium sulfate residue on the surface of acid-treated recycled fine aggregate which reacts with cement and induces a reduction in calcium silicate hydrates and promotes the setting of mortar cement. The mortars studied can be used for bonding mortars, as the setting time value is higher than 120 min, the minimum value for mortars of this utility [35].

The bonding that takes place during hydration between the cement paste and the aggregates results in a particular paste zone called the "transition aureole" or paste/aggregate interface, so the interaction between the matrix and the aggregates in this zone will depend on the physical parameters and the chemical composition of the sands.

5.7. Mechanical Test

5.7.1. Flexural strength results

The figure 9 shows the evolution of the average flexural strengths at 2, 7, and 28 days measured at room temperature.

It was found that they vary from 1.64 to 2.18 MPa at 2 days, from 3 to 3.90 MPa at 7 days, and from 7 to 14.84 MPa at 28 days. It can be seen that quarry sand mortars have higher average flexural strengths than alluvial sand mortars at 28 days, although at 2 days these strengths tend to equalize. In fact, at early age, as the cementing process is not completed, the cementitious materials tend to show the same mechanical behavior, whereas at 28 days they show an almost stable behavior over time [36]. The flexural strength performance of quarry sands is due to the angular nature of the sand grains, which favors mortars subjected to flexure compared to alluvial sand mortars, whose sand grains are generally round in shape. Similar results were obtained in the work of Kumar et al Ashok [7], where the replacement of alluvial sand with granite powder resulted in flexural tensile strengths increasing by 23-39% depending on the case.

It seems clear that the response of mortars to bending stresses is strongly dependent on the shape of the sand grains, with an angular shape favoring strength over a rounded shape. The divergence of strengths in materials of the same shape would depend on the intrinsic properties of the materials, which can be elucidated by studying the compressive strengths.

5.3.1. Compressive strength results

The test was carried out at ages of 2, 7, and 28 days of curing following NF- P- 15-301 and ENV 197 - 1. The evolution of the compressive strengths of the different mortars is given in the figure10.

The results show that the average compressive strengths vary between 6.35 to 10.83 MPa at 2 days, 7.55 to 18.96 MPa at 7 days, and 22.81 to 34.58 MPa at 28 days. The highest values are for basalt mortar (34.58 MPa), followed by granite mortar (31.28 MPa), Gneiss mortar (28.68 MPa), and alluvial sand mortars. Similar work [4] confirms that the mechanical properties of mortars with basalt aggregate have the best mechanical performance at 28 days (34 MPa), followed by alluvial sand aggregates (24 MPa), ahead of mortars with Gneiss aggregate (22 MPa). This is because basalt is a compact rock, hard, tough, and also consists of hard minerals such as olivine, plagioclase, clinopyroxene.

Regarding the alluvial sand mortars (MS04, MW05), the MS04 mortar has higher values at 2, 7, and 28 days respectively of 8.43 MPa, 16.66 MPa, 24.37 MPa than the MW05 with 6.35 MPa, 7.55 MPa, and 22.81 MPa respectively. This slight difference in favor of MS04 is due to a

higher percentage of silica, thus quartz and other hard minerals such as plagioclases (XRF and XRD results). SW05 also has a higher organic matter content (LOI = 1.87) than SS04 (LOI = 1.55), which harms the cementitious matrices [37].

Overall, these results support that the quarry sand mortars studied have higher average compressive strengths than the alluvial sand mortars. In addition, sands of volcanic origin provide better strengths than sands of metamorphic origin, with basalt providing the best performance. The quality of alluvial sands depends on their constituent minerals, their degree of weathering, and their organic matter content.

5.4. XRD results on mortars

The 28-day XRD results for the mortars studied (MB01, MGR02, MGN03, MS04, and MW05) are shown in Figure11.

These results allowed the identification of all the minerals present in the raw materials. In addition to these, the non-hydrated cementitious minerals Halite (5.88 Å; 3.88 Å; 2,70 Å; 1,94 Å 1,63 Å; 1.54 Å), Belite (4,06 Å; 3.76 Å; 3.49 Å; 3.422 Å; 3.14 Å; 2.89 Å ; 2.70 Å, 2.51 Å, 2.36 Å, 2.28 Å, 2.03 Å, 2.01 Å, 1.97 Å, 1.81 Å, 1.75 Å,), Tricalcium Aluminate, (4.23 Å; 3.42 Å; 3.35 Å; 2.78 Å; 2.20 Å; 1.88 Å; 1,56 Å, 1.35 Å) and tetracalcium alumino ferrite (3.65 Å; 2.78 Å; 1.86 Å; 1.81 Å; 1.54 Å), calcium oxide (1.45 Å; 1.38 Å) [30]. The hydrates identified are Ettringite (5.60 Å ; 4.69 Å ; 2,61 Å; 2.20 Å, 1.94 Å), CSH (9.86 Å ; 5.60 Å, 3.49 Å; 3.42 Å; 3,22 Å; 3.00 Å ; 2.51 Å; 2,16 Å; 2,11 Å; 2.03 Å; 1.94 Å, 1.83 Å ; 1.72 Å ; 1.52 Å), Portlandite (1.79 Å ; 1,48Å; 1.44 Å), Monosulfoaluminate (2.36 Å; 2.22 Å; 1.83 Å, 1.59 Å), Katoite (3.14 Å; 2,46 Å; 2.30 Å, 2.03 Å, 1.81 Å, 1.59 Å; 1.40 Å) and to a lesser extent Stratlingite (4.18 Å, 1.88 Å; 166 Å) [30]. There is an absence of transformation of the sand minerals and the hydrates formed are those found in Portland cements independently in sands. The result is that the chemical constituents of the sands do not seem to react with those of the cements, certainly due to the fact that they are mostly in a crystalline state. Indeed, amorphous materials have been shown in numerous studies [38, 39, 40], to influence the mechanical properties of cementitious matrices. For other researchers [22,9], crushed basalt on the one hand and crushed granite on the other hand, mainly influence the physical behavior of mortars.

6. Conclusion

The objective of this work was to carry out a comparative study of the physicochemical and mineralogical properties of sands of different geological natures in mortars. For this purpose, we used Canada sand and wouri sand as alluvial sands. For quarry sands, basalt, gneiss, and granite sands were used. The particle size classification of these sands showed that the granite and basalt sands had curves closest to the standard sand, the other sands had a greater amount of fines, with a predominance of fines in the Gneiss sand. Chemical analysis indicated the presence of minerals that were confirmed by petrography and mineralogy. These included muscovite, olivine, plagioclase, amphibole, biotite, quartz, kaolinite, orthoclase, vermiculite, augite, microcline, among others. These minerals corresponded to the minerals commonly found in the geological areas from which the materials used for the study were derived. The presence of hard minerals such as quartz and plagioclase was responsible for the strength of the rocks, and hence the grain sizes obtained after grinding. The analysis of the setting time of mortars showed that the presence of fine particles influenced the setting time. The higher the fine content, the longer the setting time. The initial setting time varied from 195 min for MS04 to 210 min for MGN03, via MW05 (200 min), MB01 (198 min), and MGR02 (196 min). The final setting time varied from 496 min (MGR01) to 510 min (MGN03) with an average of 300 min over and above the initial setting time to reach the final setting time. The flexural strength tests of the mortars showed that the crushed sands had better properties than the alluvial sands. They varied from 1.64 to 2.18 MPa at 2 days, from 3 to 3.90 MPa at 7 days, and from 7 to 14.84 MPa at 28 days. In the compressive stress tests, the results showed that the quarry sand mortars studied have higher average compressive strengths than the alluvial sand mortars, with basalt sand performing best. The strengths ranged from 6.35 to 10.83 MPa at 2 days, 7.55 to 18.96 MPa at 7 days, and 22.81 to 34.58 MPa at 28 days, with 34.58 MPa for the basalt mortar. These results were due to a more abundant presence of hard minerals. The mineralogical analysis of the mortars revealed the presence of cement hydrates and non-hydrated phases in all the mortars. It was also noted that there were no minerals in the sands that could chemically interfere with the setting process. The results thus obtained could be completed by studying the transition interface between the sand grains and the cement through scanning electron microscopy on the mortars. This investigation will be the subject of a future study.

Acknowledgements The authors of this article wish to acknowledge the assistance of the staff of the Laboratory at MIPROMALO in the characterization of raw materials and cement products. Part of the work was performed thanks to the support from the Laboratory of Clays, Geochemistry and Sedimentary Environments (AGEs), University of Liege, Belgium.

Author Contributions Yannick Tchedele Langollo: Validation, Methodology, Writing - review & editing, Visualization, original draft, Bilkissou Alim: Conceptualization, Methodology, Investigation, Writing - original draft. Njoya Mfokou Abdou Nasser: Validation, Writing - review & editing, Visualization... Oumar Ali Taïga: Methodology, Writing review & editing, original draft Njoya Moussa Jalil: Methodology, Investigation, review & editing, Belinga Essama Boum Raphael: Supervision, Methodology, Resources, Mache Jacques Richard: Supervision, Methodology, Resources.

Funding The authors received no financial support for the research, authorship, and/or publication of this article.

Data Availability All data generated or analyzed during this study are included in this article.

Compliance with Ethical Standards This manuscript has been published elsewhere in any form or language and has not been submitted to more than one journal for simultaneous consideration.

Declaration on Conflict of Interest The authors declare that they have no conflict of interest.
Code Availability Not applicable.
Consent to Participate Not applicable.
Consent for Publication Not applicable.

Références

[1] Mambou N. L. L. and Mvogo E. P. J. (2020) *Influence of the Mixture of Alluvial Sand and Quarry Sand as Fine Aggregate on the Physical and Mechanical Properties of Hydraulic Concrete: The Case of Alluvial Sand from the Nyong River and Crushed Sand from the Quarry of Nkoulouganga (Center, Cameroon),* European Journal of Scientific Research, ISSN 1450-216X / 1450-202X Vol. 156 No 4 June, pp.359 – 370

[2] Tchapga, G. G. M., Mambou, N. L. L., Tchoffo, F., Hamidou, G. F., Ndjaka, J. M. B. (2019). *Mechanical and physical performances of concretes made from crushed sands of different geological nature subjected to high temperatures*, Engineering Science and Technology, an International Journal, March, P. 1116–1124

[3] Ghomari, F. Bendi-ouis, A. (2008). *Science des matériaux de construction.* Université Abou Bekr Belkaid, faculté des sciences de l'ingénieur, Travaux pratique département de génie civil. 36p.

[4] Mambou, N. L. L., Tchapga, G. G. M., Ndop, J., Fofe, M. C. and Ndjaka, J. M. B. (2017) *A Comparative Study of Concrete Strength Using Metamorphic, Igneous, and Sedimentary Rocks (Crushed Gneiss, Crushed Basalt, Alluvial Sand) as Fine Aggregate*, Journal of Architectural Engineering Technology. March, DOI: 10.4172/2168-9717.1000191

[5] Dad, C. (2019*). Etude comparative de l'utilisation du sable de dune en substitution du sable de rivière : cas des mortiers normalisés*. Mémoire de fin d'études en vue de l'obtention du diplôme de Master en génie civil. Université Mouloud Mammeri de Tizi-Ouzou, Faculté de génie de la construction, Département de Génie civil. 129p.

[6] Lakhdari, M. F., Zaidi, A., Bouhicha, M., Krobba, B., (2021). *Sulfate Resistance of Cementitious Mortar Based on Dune and Alluvial Sands in Hot Region* Iranian Journal of Science and Technology, Transactions of Civil Engineering April, 45:697–706, https://doi.org/10.1007/s40996-021-00632-9

[7] Kumar, G.L. et Ashok K.V. (2018), *Impact on mechanical properties of cement sand mortar containing waste granite powder*, construction and building materials, September, P.155-164

[8] Elat, E., Pliya, P., Pierre, A., Michel, M. and Noumowé, A. (2020). *Microstructure and Mechanical Behavior of Concrete Based on Crushed Sand Combined with Alluvial Sand.* Civil Eng, September P.182-197

[9] Manasseh, J., (2010). *Use of Crushed Granite Fine as Replacement to River Sand in Concrete Production,* Leonardo Electronic Journal of Practices and Technologies, December, p. 85-96, ISSN 1583-1078

[10] Pouguininséli, M. (2016). *Etude l'influence de la qualité du sable sur les propriétés physico-mécaniques d'un béton courant.* Mémoire de master. 2iE, Ingénierie de l'eau et de l'environnement, option génie civil. 61p.

[11] Bechiri, F. (2011). *Effet de la nature du sable sur le comportement des mortiers.* Mémoire de magister. Université e Guelma, Faculté des sciences et de l'ingénierie, Département de génie civil, Matériaux et structure. 116p.

[12] Lassere, M., (1961). *Carte Géologique de Reconnaissance à l'échelle du 1/500 000. Territoire du Cameroun, Ngaoundéré Est*. Dir. Mines Géol. Cameroun, Yaoundé, 1 carte et notice.

[13] Toteu S.F., Penaye J., Deschamps Y., Maldan F., Nyama Altbagoua B., Bouyo Houketchang M., Sep Nlomgam J.P., Mbola Dzana S.P., (2008). *Géologie et ressources minérales du Cameroun*, 33rd International Geological Congress, Oslo, Norway, August, P. 6-14.

[14] Tchameni R., Pouclet A., Penaye J., Ganwa A.A., Toteu S.F., (2006). *Petrography and géochemistry of the Ngaoundéré Pan-African granitoïds in Central Nord-Cameroon: implication for their sources and geological setting*. Journal of African Earth Sciences 44, Pp. 511-529.

[15] Ganwa, A. A., Wolfgang, F., Wolfgang, S., Ekodeck, G.E.,Kongyuy S., Ngako, V., (2008). *Archean inheritances in the pyroxène–amphibole bearing gneiss of the Meiganga area (Central North Cameroon): Geochemical and 207Pb/206Pb age imprints*. Comptes Rendus Geosciences 340, N°4, Pp. 211-222.

[16] Touteu, S. F., Van Schmus, W. R., Penaye J., Nyobe J. B., (1994). U-Pb and SmNd evidence for erburniam and Pan-African high-grade metamorphism in cratonic rock of southern Cameroon. Precambrian Res., 67, Pp 321- 347.

[17] Vicat, J. P., (1998). *Esquisse géologique du Cameroun. In Géoscience au Cameroun*, Vicat, J. P. et Bilong, P. éd. Collect. GEOCAM, Vol. 1, Press. Univ. Yaoundé I pp 3- 11.

[18] Nkoue Ndongo G. R., (2008). *Le cycle du carbone en domaine tropical humide : Exemple du bassin versant forestier du Nyong au Sud Cameroun*, Thèse Doct. Univ. Yaoundé I, 279p.

[19] Owona, S., Ondoa Mvondo, J., Essono, j., Njom, B., Emana Mengong, M., 2003. Géomorphologie et cartographie de deux faciès paradérivées et orthodérivées de la région de Yaoundé, vol. 10, N° 1 pp 81-91.

[20] Dubreuil P, Gustave J, Nouvelot F, Olivry C. (1975*). Monographies hydrogéologiques ORSTOM N°3, le bassin versant de la rivière Sanaga*. Office de la recherche scientifique et technique Outre-mer. 431p.

[21] Olivry C. (1974). *Régime hydrologique du fleuve Wouri et estimation des apports reçus par l'estuaire du Wouri.* Office de la recherche scientifique et technique Outre-mère. 60p.

[22] Uncik, S. and Kmecova, V. (2013) The effect of basalt powder on the properties of cement composites, Procedia Engineering. P.51-56 doi: 10.1016/j.proeng.2013.09.010

[23] Pavlovic, M., Dojcinovic, M., Prokic-Cvetkovic, R., Ljubisa, A. (2019). *The Mechanisms of cavitation erosion of raw and sintered Basalt*, Science of Sintering, Pp. 409-419

[24] Dobiszewska, M., Beycioğlu, A. (2017) *Investigating the Influence of Waste Basalt Powder on Selected Properties of Cement Paste and Mortar*, Materials Science and Engineering, doi:10.1088/1757-899X/245/2/022027

[25] Gougazeh, M., Bamousa, A., and Hasan, A. (2018) *Evaluation of granitic rocks as feldspar source: Al Madinah, Western Part of Saudi Arabia*, Journal of Taibah University for Science, 12:1, Pp.21-36, DOI: 10.1080/16583655.2018.1451111

[26] Boone, M., Dewanckele, J., Marijn, B., Cnudde, V., Silversmit, G., Ranst, E. V., Jacobs, P., Vincze, L., and Hoorebeke1, L.V., (2011) *Three-dimensional phase separation and identification in granite,* Geosphere, DOI: 10.1130/GES00562.1

[27] Padhi1, J. k., Kumar, A M., Sadasiba, J. and Senthil, K.G.R., (2017) *geochemical and mineralogical studies of crystalline limestone occurred near podupatti village of ettayapuram*

taluk, tamil nadu, International Journal of Latest Trends in Engineering and Technology, Vol. (8) Issue (2), pp.280-288, DOI: http://dx.doi.org/10.21172/1.82.037

[28] Bozkaya, O., Yalcin, H., Basibuyuk, Z., and Bozkaya, G., (2007). *metamorphic-hosted pyrophyllite and dickite occurrences from the hydrous al-silicate deposits of the Malatya-Puturge region, central-eastern Anatolia, Turkey,* Clays and Clay Minerals, Vol. 55, No. 4, Pp.423–442, DOI: 10.1346/CCMN.2007.0550409

[29] Tchapga, G. M. G., Mambou, N. L. L., Foguieng, W. M., and Ndjaka, B. J. M. (2020). *Microstructure analysis of hydraulic concrete using crushed basalt, crushed gneiss and alluvial sand as fine aggregate. JMST Advances*, *2*(2), 25–35. https://doi.org/10.1007/s42791-020-00031-7

[30] Ndjigui, P.D., Onana, V.L., Sababa, E., Bayiga, E. C. (2018), *Mineralogy and geochemistry of the Lokoundje alluvial clays from the Kribi deposits, Cameroonian Atlantic coast: Implications for their origin and depositional environment*, Journal of African Earth Sciences, DOI: 10.1016/j.jafrearsci.2018.03.023

[31] Katz, A., Kulisch, D., (2017). Performance of mortars containing recycled fine aggregate from construction and demolition waste. Mater. Struct. 50 (4), 199.

[32] Munoz-Ruiperez, C., Rodriguez, A., Gutierrez-Gonzalez, S., Calderon, V., (2016). Lightweight masonry mortars made with expanded clay and recycled aggregates. Constr. Build. Mater. 118, 139e145.

[33] Resende, C., Cachim, P.B., Bastos, A.M., (2008). Copper slag mortar properties. In: In Materials Science Forum Trans Tech Publications, 587, pp. 862e866.

[34] Kim, H.K., Ha, K.A., Lee, H.K., (2016). Internal-curing efficiency of cold-bonded coal bottom ash aggregate for high-strength mortar. Constr. Build. Mater. 126, 1e8.

[35] Buyuksagis, I.S., Uygunoglu, T., Tatar, E., (2017). Investigation on the usage of waste marble powder in cement-based adhesive mortar. Constr. Build. Mater. 154, 734e742.

[36] Newmann J, Choo BS (2003) *Advanced concrete technology, constituent materials.* Department of Civil Engineering Imperial College, Elsevier, London, p 280 **(ESBN 07506511032)**

[37] Moriyohi, A., Shibata, E., Natsuhara, M., Sakai, K., Kondo, T., Kashara, A. (2021). *Deterioration of modern concrete structures and asphalt pavements by respiratory action and trace quantities of organic matter*. PloS ONE 16(5):e0249761. Doi:10.1371/journal.pone.0249761

[38] Tchedele, L. Y., Mambou, N. L. L., Kamga, S. L. V. E., Tchamba, A. B., Ngounouno, I. and A. Bier Thomas (2020). *Mechanical and Microstructural properties of Cameroonian CPJ NC CEM II/B-P 42.5R cement substitution by glass powder in the cement paste and mortar*. SN applied Science. 2:1368. P.12. https://doi.org/10.1007/s42452-020-3152-y.

[39] Prokopski G, Halbiniak J (2000) Interfacial transition zone in cementitious materials. Cem Concr Res 30(4):579–583

Figures

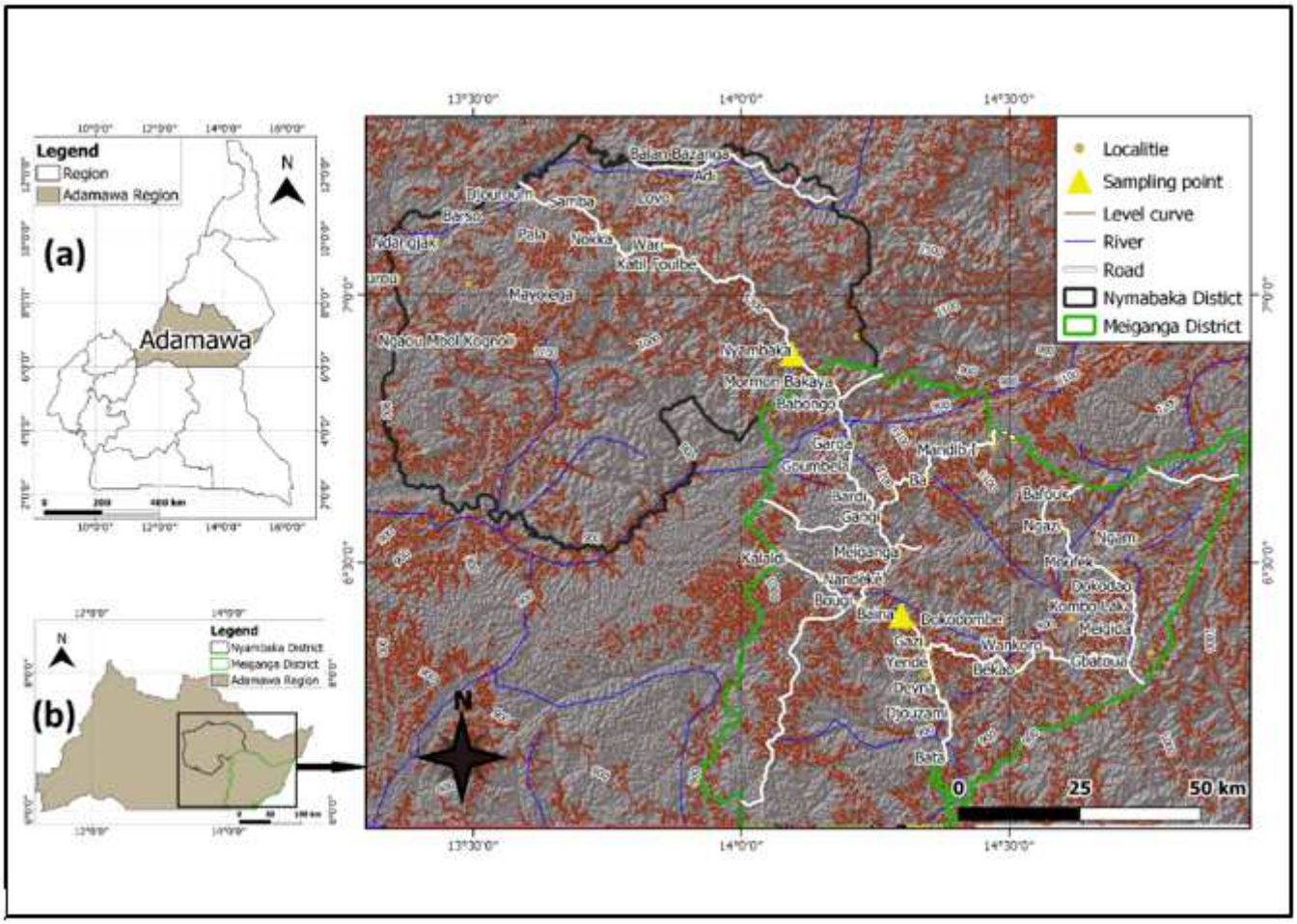

Figure 1

Location of the study area in the Adamaoua region

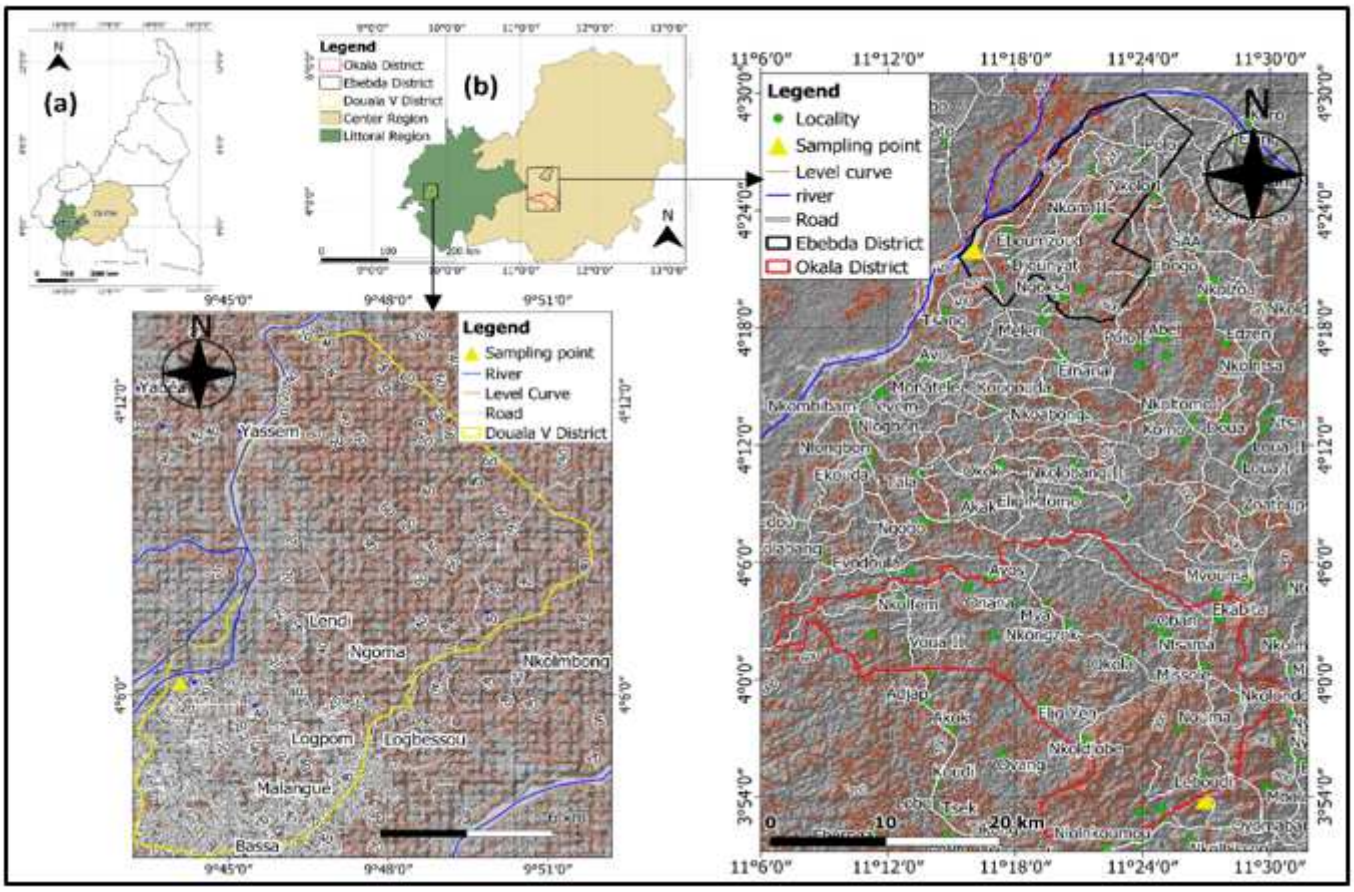

Figure 2

Location of study areas in the central and littoral regions

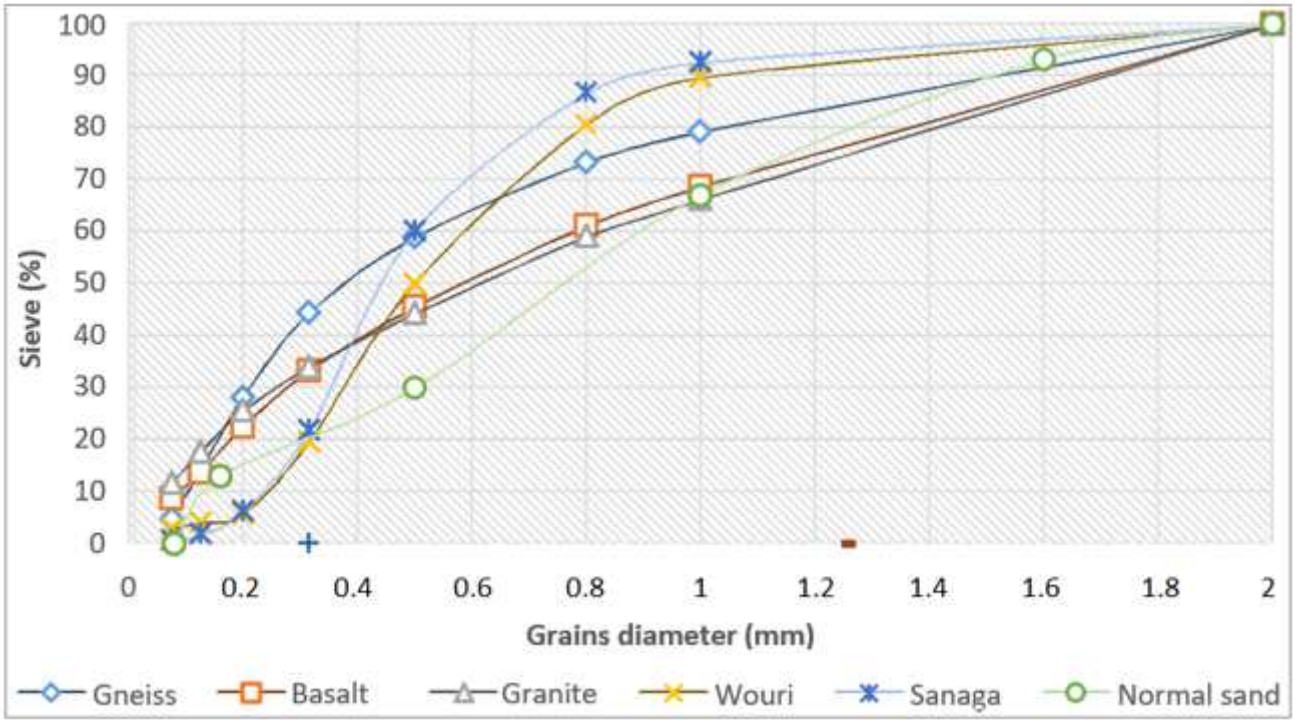

Figure 3

sand grading curves

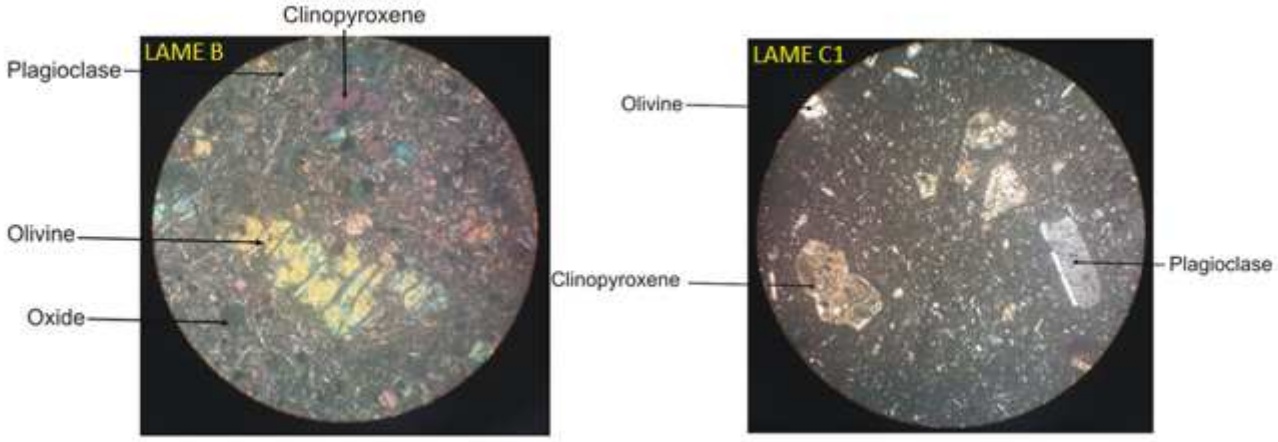

Figure 4

Photomicrograph of basalt (LAME B and LAME C2) as seen under cross-polarized light (LPA).

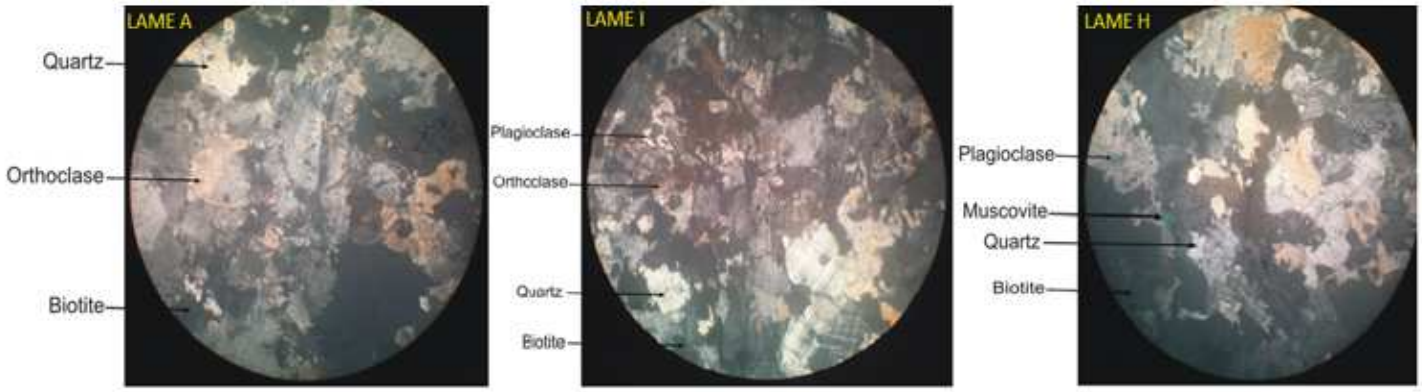

Figure 5

Photomicrograph of granite (LAME A, LAME I, and LAME H) as seen under cross-polarized light (LPA).

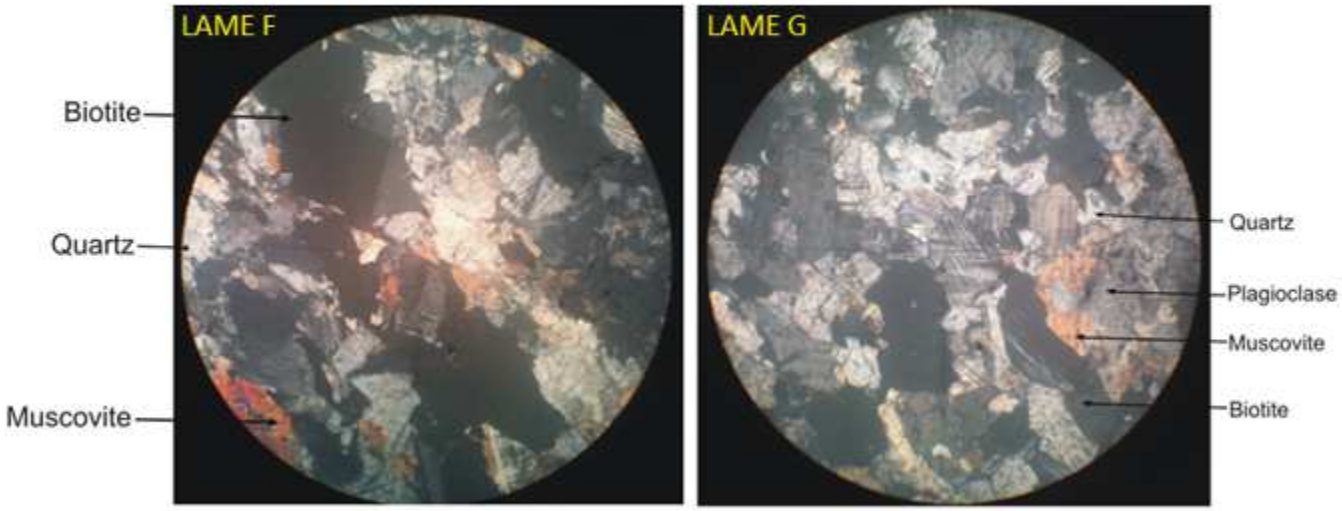

Figure 6

Photomicrograph of gneiss (LAME F and LAME G) as seen under cross-polarized light (LPA).

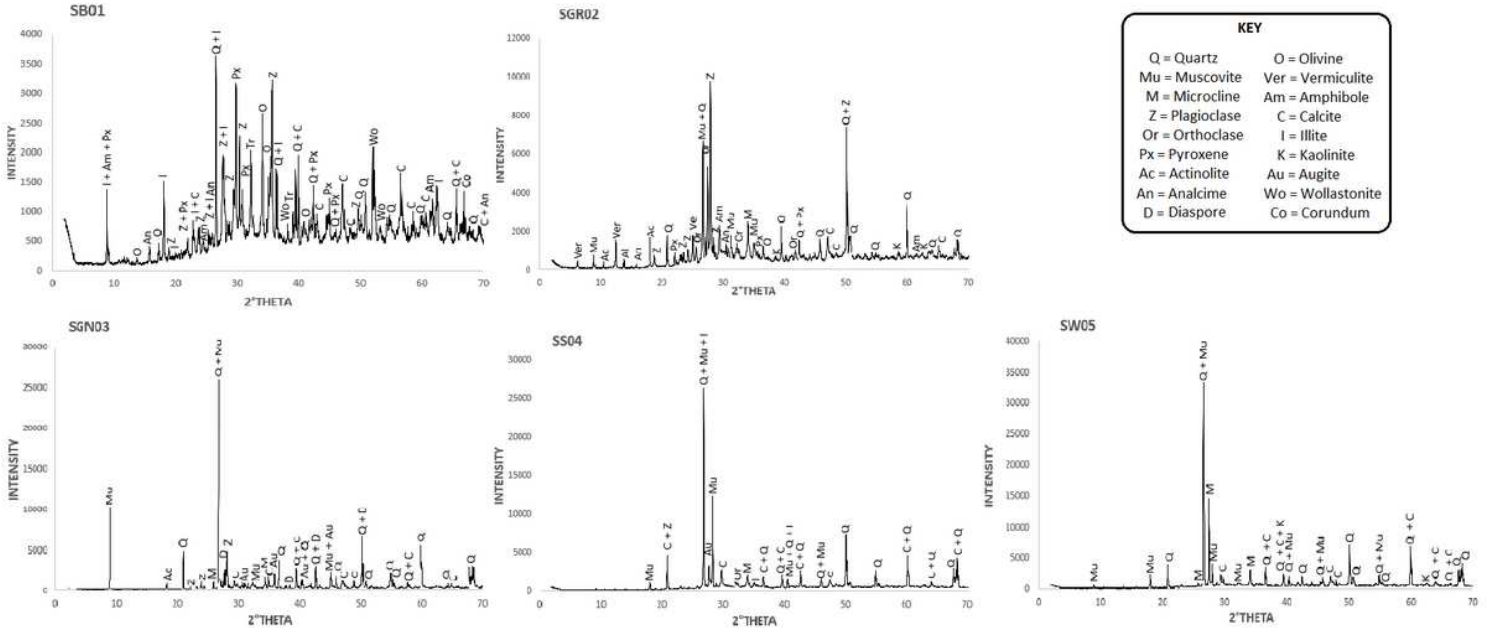

Figure 7

XRD on raw materials SB01, SGR02, SGN03, SS04, and SW05

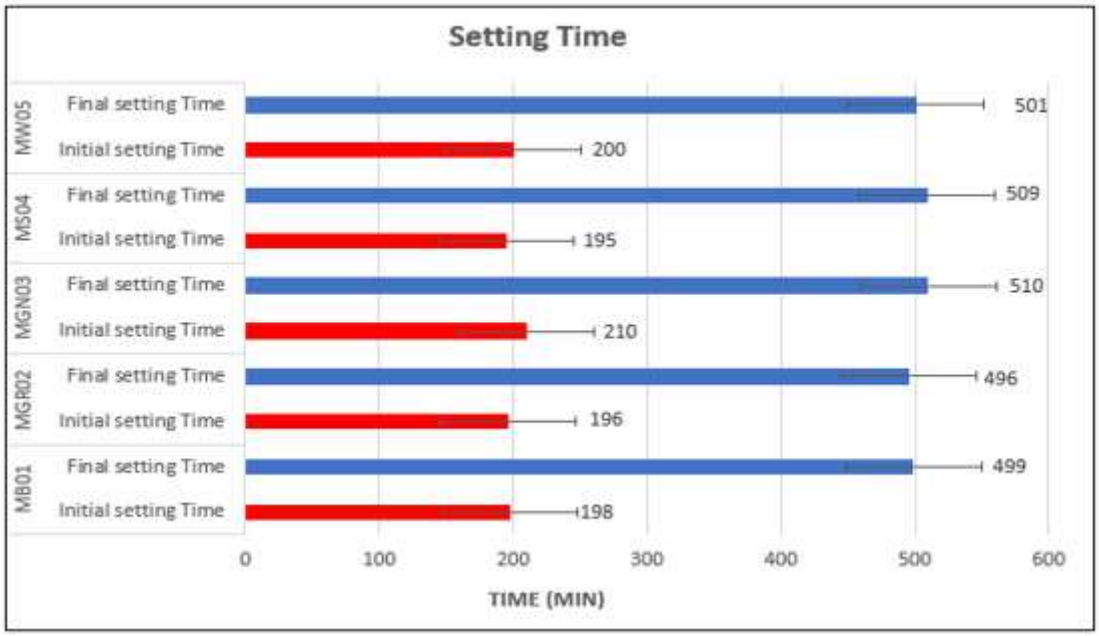

Figure 8

Setting time results

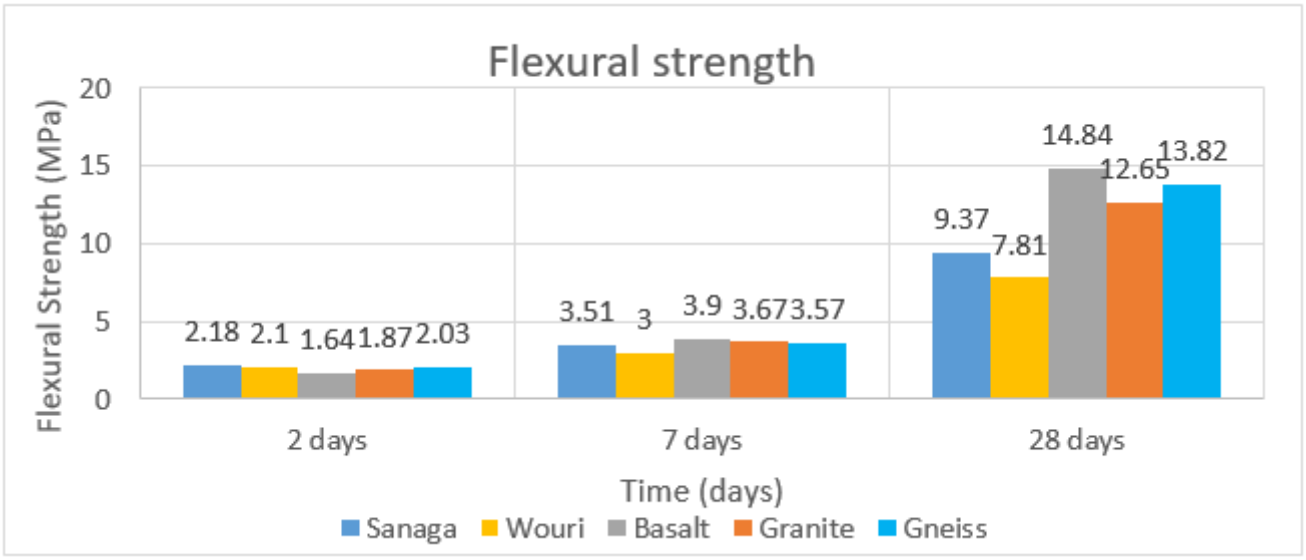

Figure 9

Flexural strength of mortars

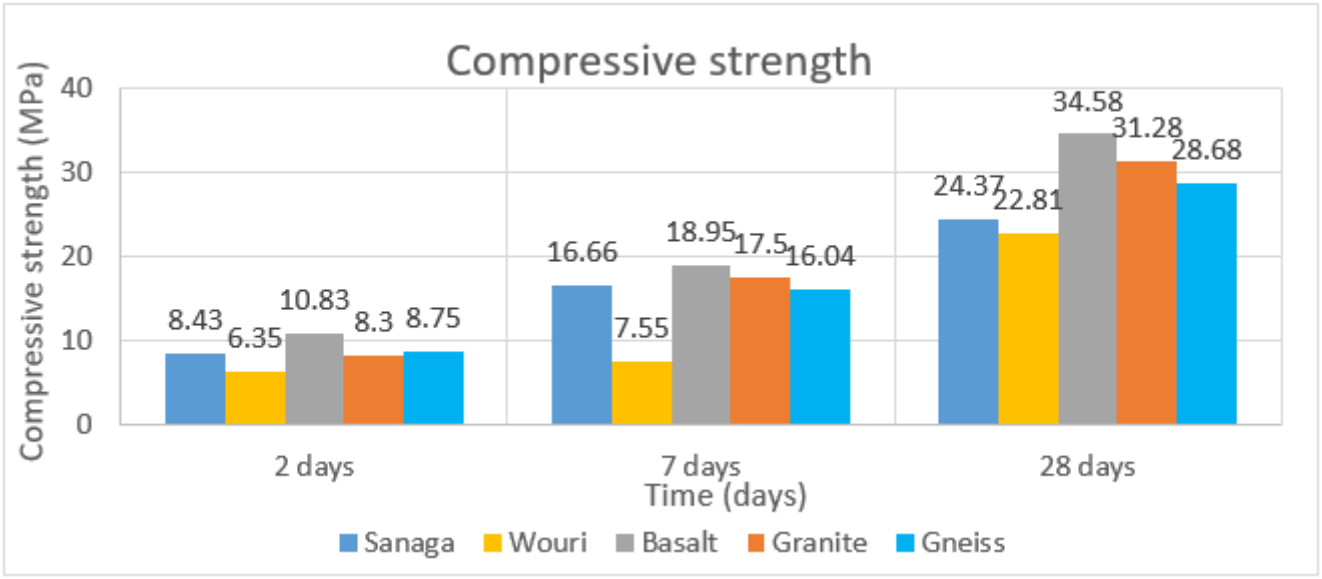

Figure 10

Compressive strength of mortars

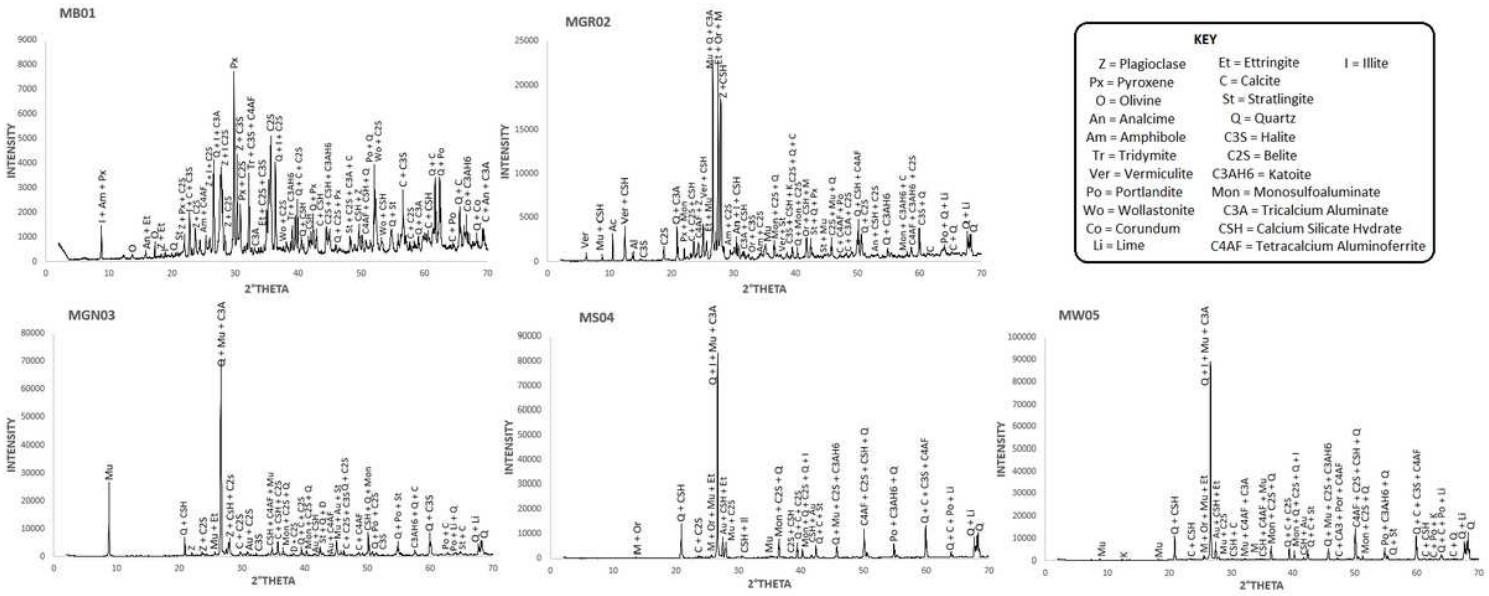

Figure 11

XRD on mortars MB01, MGR02, MGN03, MS04, and MW05